Journal of Solid State Chemistry 182 (2009) 1700–1707

Contents lists available at ScienceDirect

Journal of Solid State Chemistry

journal homepage: www.elsevier.com/locate/jssc

Growth of ordered silver nanoparticles in silica film mesostructured with a triblock copolymer PEO–PPO–PEO

L. Bois [a,*], F. Chassagneux [a], S. Parola [a], F. Bessueille [b], Y. Battie [c], N. Destouches [c], A. Boukenter [c], N. Moncoffre [d,*], N. Toulhoat [d,e]

[a] Laboratoire Multimatériaux et Interfaces, UMR CNRS 5615, Bat Berthollet, Université Claude Bernard Lyon 1, 43 Bd 11 nov 1918, 69622 Villeurbanne, France
[b] Laboratoire des Sciences Analytiques, UMR CNRS 5180, Bat Raulin, Université Claude Bernard Lyon 1, 43 Bd 11 nov 1918, 69622 Villeurbanne, France
[c] Laboratoire Hubert Curien, UMR 5516 – Université Jean Monnet, 18 Rue Prof. B. Lauras, Bat F, F-42000 Saint-Etienne, France
[d] Université Lyon 1, IPNL, CNRS/IN2P3, 4 rue E. Fermi, 69622 Villeurbanne cedex, France
[e] CEA/DEN, Centre de Saclay, 91191 Gif sur Yvette Cedex, France

ARTICLE INFO

Article history:
Received 17 July 2008
Received in revised form
12 January 2009
Accepted 26 January 2009
Available online 18 April 2009

Keywords:
Silver nanoparticles
Block copolymer
Silica film

ABSTRACT

Elaboration of mesostructured silica films with a triblock copolymer polyethylene oxide–polypropylene oxide–polyethylene oxide, (PEO–PPO–PEO) and controlled growth of silver nanoparticles in the mesostructure are described. The films are characterized using UV–visible optical absorption spectroscopy, TEM, AFM, SEM, X-ray diffraction (XRD) and Rutherford backscattering spectrometry (RBS). Organized arrays of spherical silver nanoparticles with diameter between 5 and 8 nm have been obtained by $NaBH_4$ reduction. The size and the repartition of silver nanoparticles are controlled by the film mesostructure. The localization of silver nanoparticles exclusively in the upper-side part of the silica-block copolymer film is evidenced by RBS experiment. On the other hand, by using a thermal method, 40 nm long silver sticks can be obtained, by diffusion and coalescence of spherical particles in the silica-block copolymer layer. In this case, migration of silver particles toward the glass substrate-film interface is shown by the RBS experiment.

1. Introduction

The development of silver nanoparticles arrays has a significant importance [1] since they have potential applications in the fields of optics [2,3], catalysis [4], and biomedicine [5]. Silver nanoparticles have unique optical properties coming from the collective oscillation of conduction electrons in case of interaction with an electromagnetic wave, which is called surface plasmon resonance (SPR). The SPR depends on the dielectric constant of the medium, on the size and the shape of nanoparticles. In case of assemblies of metallic nanoparticles, the surface plasmon resonance can be strongly modified [6,7].

We are interested in the fundamental aspects of the role of the organization, size and shape of metallic nanoparticles on SPR phenomena. New methods for controlling the growth of nanoparticles using mesostructured sol–gel films are developed and results on hybrid silica based on copolymer PEO–PPO–PEO are presented in this paper.

Block copolymers form micelles and regular self-assembled nanostructures are easily obtained. These nanostructures can be used as reactors for the synthesis of metallic nanoparticles [8–15]. The spatial organization of the metallic nanoparticles is then determined by the block copolymer organization. On the other hand, block copolymer are chemically selective, since their different blocks will present various coordination properties with metallic ions. For instance, the amphiphilic PEO–PPO block copolymer has been shown to act as the same time as reducing, stabilizing and a morphogenic agent in the growth of silver nanoparticles in solution [14]. The hydrophilic PEO block can slowly reduce Ag^+ ions to Ag, at room temperature, resulting in the oxidation of the oxyethylene groups [15].

There are a lot of studies concerning the growth of silver nanoparticles inside a silica film, obtained either by the sol–gel process [16–28] or by atom-beam sputtering [29–32]. Mesostructured silica, elaborated by hydrolysis and condensation of a silica precursor with amphiphilic compounds, such as surfactants or block copolymers, have also been recently considered as template for the synthesis of silver nanoparticles in silica films [33–46].

The formation of silver nanoparticles using in situ reduction with $NaBH_4$ or thermal reduction in a mesostructured silica film is reported in this article. A mesostructured silica film with a

* Corresponding authors. Fax: +33 4 72 44 06 18.
E-mail addresses: laurence.bois@univ-lyon1.fr (L. Bois), n.moncoffre@ipnl.in2p3.fr (N. Moncoffre).

0022-4596/$ - see front matter © 2009 Elsevier Inc. All rights reserved.
doi:10.1016/j.jssc.2009.01.044

triblock copolymer PEO–PPO–PEO, F127 [47,48] is used and a one step process is followed for the synthesis of nanoparticles, introducing silver salt during the first stage of the mesostructured film synthesis.

2. Experimental part

2.1. Materials

Silver nitrate ($AgNO_3$), sodium borohydride ($NaBH_4$), tetraethoxysilane (TEOS, $Si(OEt)_4$), block copolymer F127 ($(PEO)_{106}(PPO)_{70}(PEO)_{106}$) is purchased from Aldrich.

2.2. Mesostructured silica films

The silica sol is prepared by hydrolyzing TEOS in the presence of the F127 block copolymer $(PEO)_{106}(PPO)_{70}(PEO)_{106}$. F127 (1.14 g) is dissolved in EtOH (11.8 g). Silica sol is prepared from TEOS (4 g) by adding an acid solution containing nitric acid at 0.055 M (1.76 g)

The sol is stirred for half an hour and the block copolymer solution F127 is added [47,48]. Silver salt is then added by using 5% or 20% doping (the atomic ratio Ag/Si ratio is considered). The mixture is stirred for half an hour at room temperature. Films are prepared by dip-coating on cleaned glass slides. A 20 mm/min dip-coating rate is used. The film is then dried at room temperature for 24 h.

2.3. Silver nanoparticles on mesostructured silica films

Reduction of silver proceeds either through immersion of the mesostructured silica films for 1 min into a freshly prepared sodium borohydride solution (50 mM), rinsed in water and dried at 100 °C, or through a thermal treatment at 200 °C (rate 1 °C/min and 2 h stage at 200 °C). Samples are called Fag5Si and Fag20Si. The term d2 or NaB refers, respectively, to a thermal treatment at 200 °C or to a chemical reduction with $NaBH_4$ solution. The as-synthesized samples Fag5Si and Fag20Si, before the reductive treatment, are colorless. The three samples Fag5SiNaB, Fag5Sid2 and Fag20SiNaB present a yellow coloration, while the Fag20Sid2 sample presents a blue coloration (Fig. 1).

2.4. Characterization

UV–visible optical absorption spectra are recorded on a Nicolet Instrument. The TEM images are taken with a TOPCON EM002B transmission electron microscope operating at 200 kV. Samples for the TEM measurement are supported on a holey carbon-coated copper grid. The morphology of the initial and final materials is observed with a scanning electron microscope (Hitachi S800) operating at 15 kV. AFM pictures are recorded on a Picoplus (Molecular Imaging) instrument with a Si tip in tapping mode. Small-angle powder X-ray diffraction patterns are recorded using a Philipps Xpert Pro diffractometer equipped with a monochromator, using Cu $K\alpha$ radiation.

Rutherford backscattering spectrometry (RBS) is performed on the 4 MV Van de Graaff accelerator of the IPNL (Institut de Physique Nucléaire de Lyon), delivering a 2 MeV helium beam. The He^+ backscattered particles are detected at a 172° angle. The beam intensity is set at 22 nA. The SIMNRA program is used to simulate the energy spectra and to determine the atomic concentration profiles [49].

3. Results

UV–visible optical absorption spectra are presented in Fig. 2. For the two Fag5Si samples, a visible absorption band is noted at 430 nm, which is characteristic of the surface plasmon resonance of spherical silver nanoparticles. The absorbance is higher (0.45) in the case of the Fag5SiNaB than in the case of the Fag5Sid2 (0.10). The visible absorption spectrum of the Fag20SiNaB sample consists also in a band at 430 nm with a 0.71 absorbance. It may be seen that the Fag20Sid2 sample, exhibits a very broad absorption band with a maximum at 510 nm and with a 0.74 absorbance.

In Fig. 3, we present TEM images of the Fag5Si samples. In the case of the Fag5SiNaB (Fig. 3a), silver nanoparticles with a homogeneous distribution between 5 and 7 nm and with a spherical shape are observed. These particles are not distributed randomly but are located along the mesostructure line with regular intervals of about 14 nm from two respective centres of neighbouring nanoparticles.

The TEM images of the Fag5Sid2 sample (Fig. 3b) show some spherical silver particles with diameter comprised between 8 and 12 nm. The density is far below what is observed with the Fag5SiNaB sample. The nanoparticles seem also more or less randomly dispersed in the matrix.

Fig. 3 also shows the TEM images of the two Fag20Si samples. The alignment of spherical silver nanoparticles is also clearly observed for the Fag20SiNaB (Fig. 3c) (similarly to Fag5SiNaB), with size between 6 and 8 nm. On the other hand, the images of the Fag20Sid2 (Fig. 3d) reveal the formation of silver sticks with a

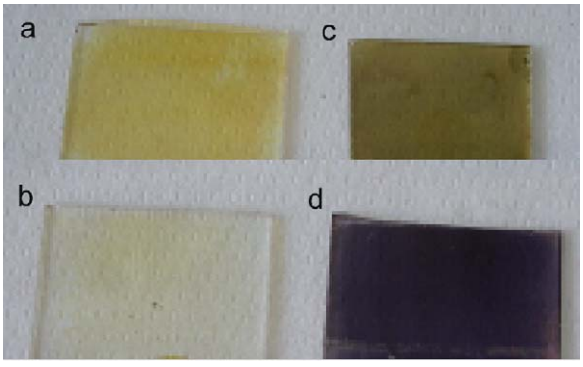

Fig. 1. Photos of the F127-silver-silica films. a: Fag5SiNB; b: Fag5Sid2; c: Fag20SiNB; d: Fag20Sid2.

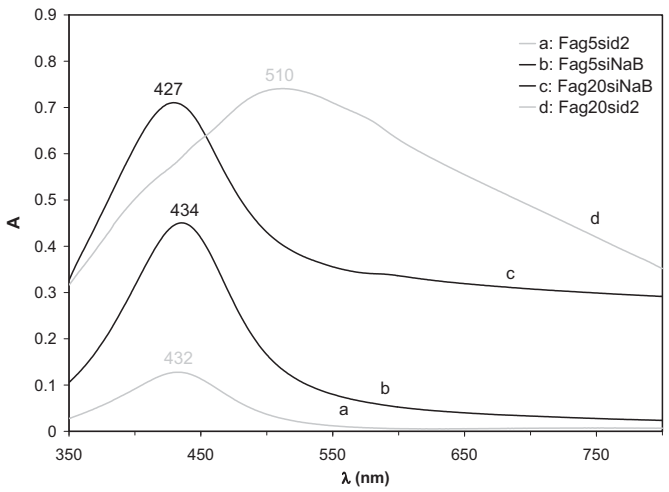

Fig. 2. UV–vis absorption spectra of F127-silver-silica films. a: Fag5Sid2; b: Fag5SiNB; c: Fag20SiNB; d: Fag20Sid2.

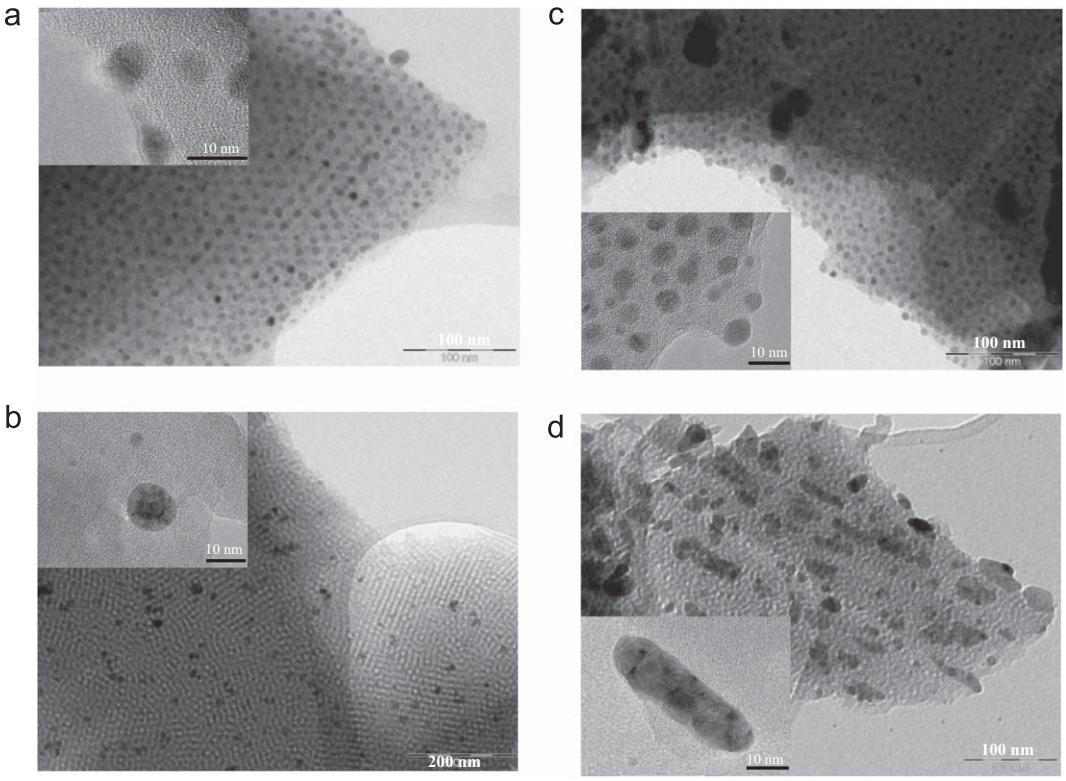

Fig. 3. TEM images of F127-silver-silica films with 5% silver. a: Fag5SiNB; b: Fag5Sid2; c: Fag20SiNB; d: Fag20Sid2.

longitudinal sizes of about 40 nm and a transversal size of about 10 nm. They are probably formed by the coalescence along a line of few spherical nanoparticles, generally about four. Moreover, these sticks have a common orientation. The sticks orientation occurs with respect to the mesostructure of the silica-block copolymer.

SEM images of the different samples are presented in Fig. 4. Before any reductive treatment, the film Fag5Si is covered with aggregates of about 30 nm (Fig. 4). After a $NaBH_4$ treatment, the formation of long aggregates of 200 nm in length is noted, while the surface is homogenously covered with smaller aggregates of 15 nm diameter. The surface of the Fag5Sid2 is very similar to that of Fag5Si, with 30 nm aggregates dispersed on the film; the density of these particles is slightly decreased with respect to Fag5Si. For a silver concentration of 20%, the surface states before and after thermal treatment are similar and characterized by the presence of 30 nm aggregates, with a higher density before than after the thermal treatment. But the surface obtained after the chemical treatment is strongly modified, with the formation of very large silver aggregates of about 100–200 nm. These large aggregates are constituted of smaller units of about 50 nm size.

AFM images (Fig. 5) confirm the results obtained by SEM since the surface of the Fag20Si sample before any treatment is covered with some particles of diameter around 60 nm. After a $NaBH_4$ treatment, a much higher density of particles of size about 50–80 nm is noted. These particles seem to be aggregated along strings. After the thermal treatment, some elongated nanoparticles (length 100 nm and width between 25 and 50 nm) are observed on the substrate which shows a 50 nm long fissuration. The density of particles is lower than the one observed before the thermal treatment.

Small-angle X-ray diffraction patterns of samples after chemical or thermal treatment are shown in Fig. 6. Samples with 0% and 1% silver nitrate are also considered for comparison. After a chemical or thermal treatment, a shoulder at respectively 0.8° or 0.9° is noted for a 0% silver salt concentration. Its intensity decreases when silver salt concentration increases and its position is shifted to higher angles. For a 20% silver salt, the diffraction feature has almost disappeared. It seems that the introduction of silver salt decreases the mesostructure organization along the direction perpendicular to the substrate and leads to a contraction of the film. This contraction is larger after thermal than chemical treatment. Without silver, as there is a single diffraction reflexion, it is not possible to propose a clear indexation without any ambiguity. Nevertheless, we believe that the mesostructuration is probably close to a cubic Im3 m one and that the observed single reflexion could be then indexed as (110) [50,51]. The results obtained for a silver salt concentration of 5% are difficult to explain. After the chemical reduction, several diffraction peaks are noted at 0.90°, 0.98° and 1.13°. The X-ray diffraction pattern becomes more complex, as if a mixture of different phases or different contraction amplitudes was present. In the case of thermal treatment, diffraction peaks are less intensive and shifted to higher angles showing the mesostructure contraction. A SAXS experimentation will be the object of a further paper to make an unambiguous interpretation of the influence of silver on the mesostructure organization.

X-ray diffraction patterns (Fig. 7) confirm the formation of metallic silver in the 20% silver salt concentration. The appearance of diffraction peaks at 2θ equal to 38.4° and 43.3°, is attributed to the (111) and (200) Bragg's reflections of the face-centered cubic structure of metallic silver [52]. For a silver salt concentration of 5%, metallic silver formation is not detected.

Experimental RBS spectra are shown in Fig. 8. The spectrum of the Fag5Si sample displays a rather large silver profile, at the film surface. After reduction with $NaBH_4$, the silver signal differs strongly from that of the initial state Fag5Si. The silver peak appears more intense and narrow, which means that a silver enrichment has occured at the film surface. The spectrum of the thermally treated Fag5Sid2 sample reveals a significant migration

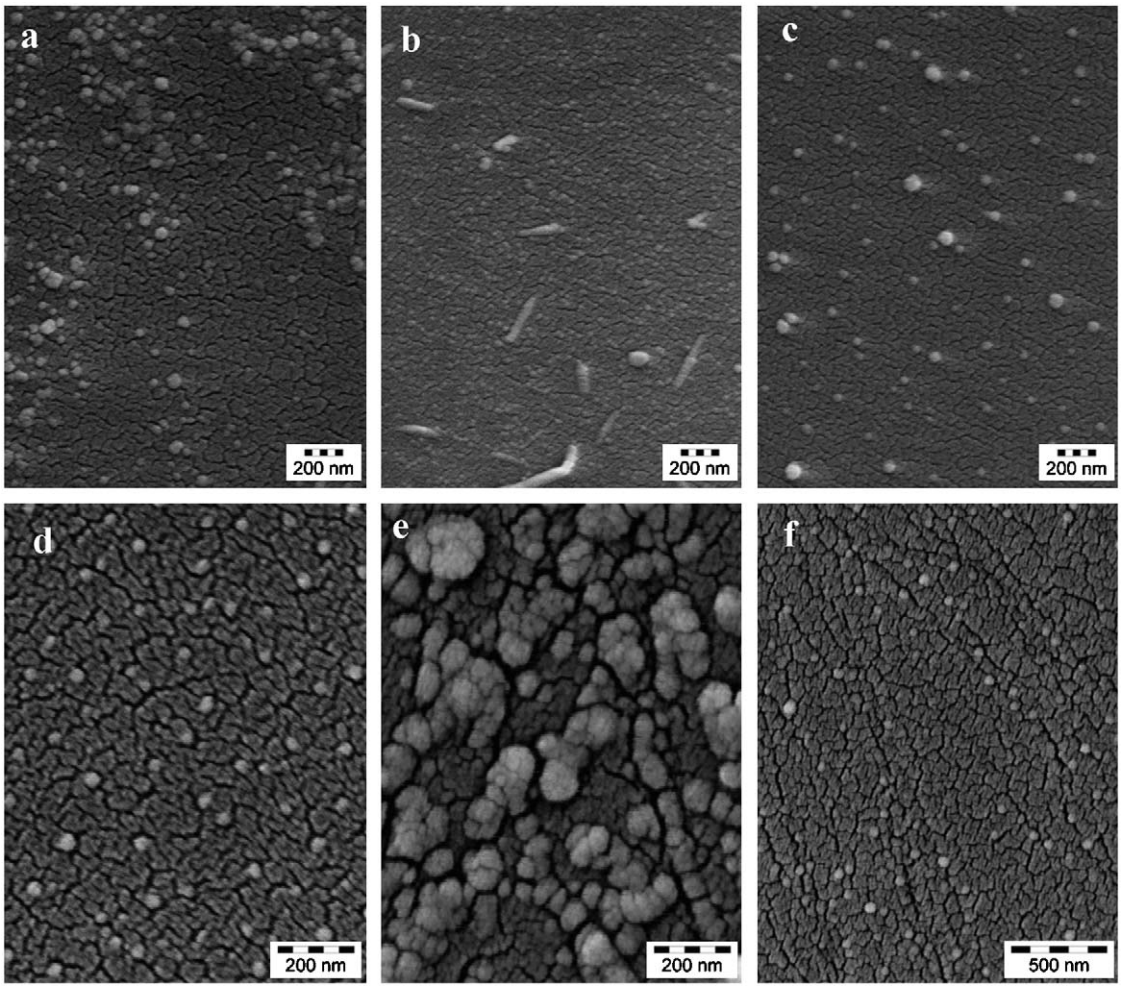

Fig. 4. SEM images of F127-silver-silica films. a: Fag5Si; b: Fag5SiNB; c: Fag5Sid2; d: Fag20Si; e: Fag20SiNB; f: Fag20Sid2.

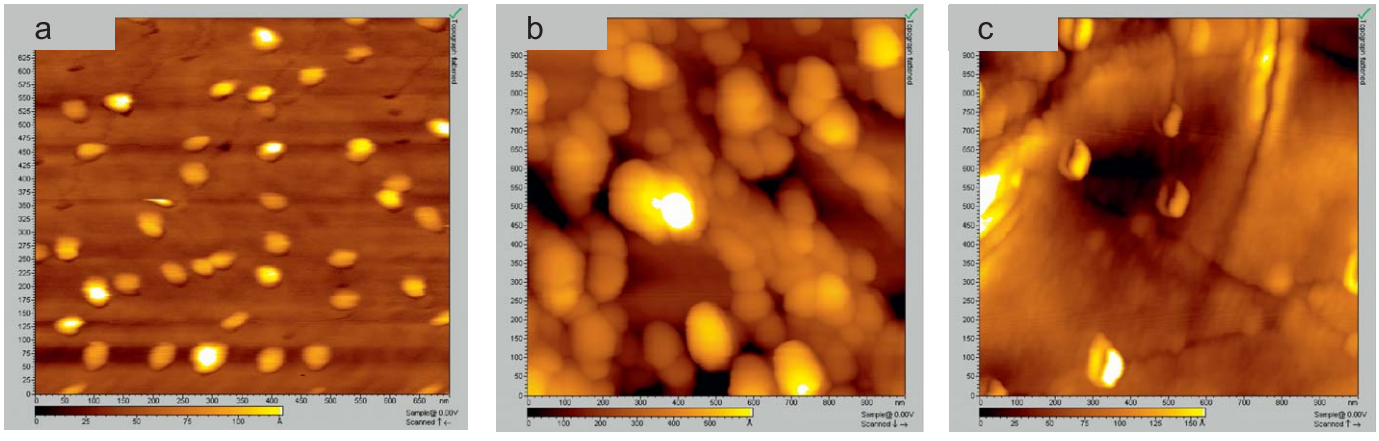

Fig. 5. AFM images of F127-silver-silica films. a: Fag20Si; b: Fag20SiNB; c: Fag20Sid2.

of silver toward the glass substrate. The same observations can be made with the spectra of the sample prepared with 20% silver salt. The $NaBH_4$ treatment leads to the migration of silver toward the film surface, while the thermal treatment results in a silver migration toward the glass substrate.

The silver profiles as function of depth are presented in Fig. 9. Silver profiles have been deducted from the RBS spectra, using the SIMNRA software. These simulations allow measuring a silver atomic concentration of 1.25% which is in good agreement with the theoretical value (1.30%) calculated from the formula $SiAg_{0.05}O_2C_{0.8}$. The calculated film thickness of Fag5Si is of 165 nm (Fig. 9a). In the case of Fag20Si, the silver atomic concentration is of 4.80%, also coherent with the theoretical value of 5% from the formula $SiAg_{0.2}O_2C_{0.8}$. The calculated film thickness is of 180 nm. As shown by the silver profile (Fig. 9) and by the schematic representation in Fig. 10, after a chemical reduction with $NaBH_4$ (in Fag5SiNB sample), most of silver (85%) is concentrated in the first 15 nm of the layer, while the rest of the layer is almost

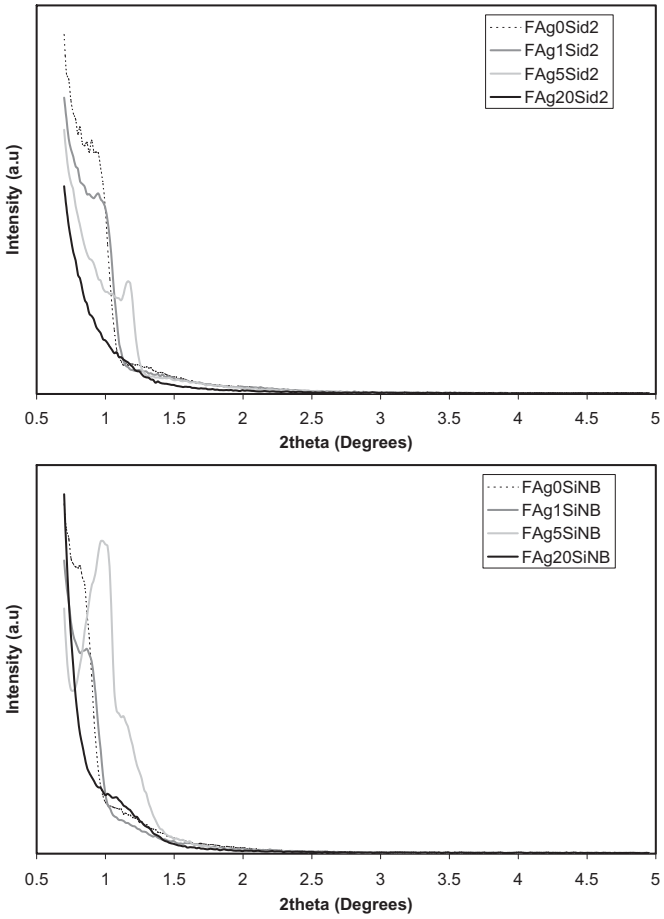

Fig. 6. Low-angle XRD patterns of F127-silver-silica films.

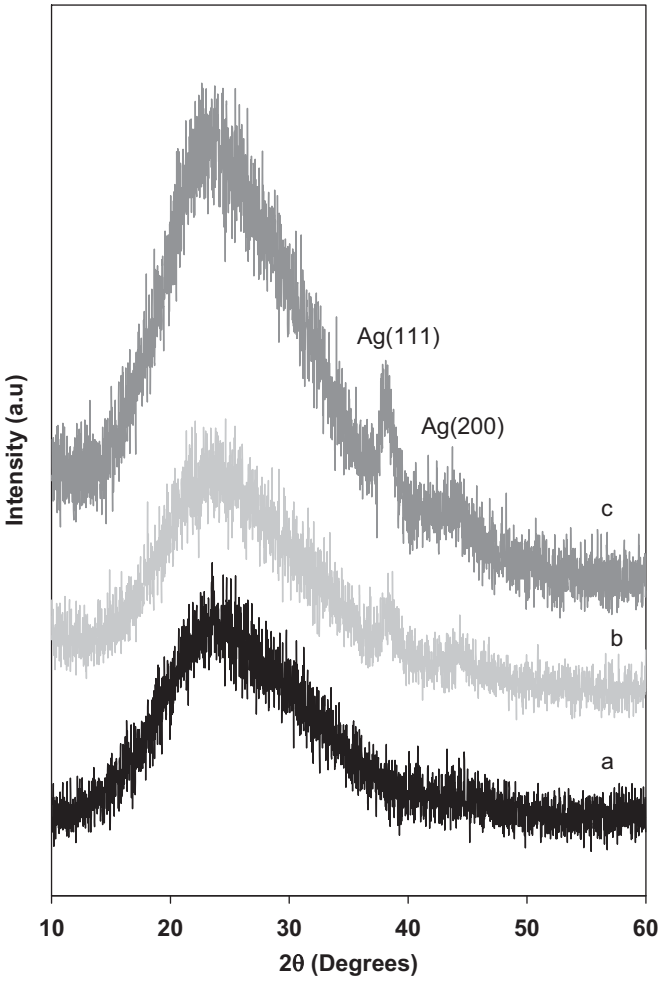

Fig. 7. Wide-angle XRD patterns of F127-silver-silica films. a: Fag20Si; b: Fag20Sid2; c: Fag20SiNB.

completely empty of silver. After a thermal treatment at 200 °C, in Fag5Sid2 sample, the silver profile is not so strongly modified, with respect to the untreated one, except that a part of silver has migrated into the glass substrate on about 400 nm depth. The thermal migration of silver from a silica film toward the glass substrate has already been evidenced by RBS experiments [53]. Similar evolution is observed for the Fag20Si sample, since after the chemical reduction, 86% of silver is concentrated in the first 12 nm of the layer; after the thermal treatment, silver migration toward the glass substrate is observed on about 400 nm depth. The silver behaviour during the chemical and the thermal processes is schematically represented in Fig. 10. The repartition of ionic silver is almost homogeneous before any reductive treatment (Fig. 10a). Ionic silver is most probably localized in the hydrophilic part of the micelle, which is the polyethylene oxide chain. After the $NaBH_4$ reduction, silver nanoparticles are localized in the first 10 nm of the layer (Fig. 10b). After the thermal process, the silver nanoparticles are dispersed within the all layer depth (Fig. 10c); a small part of silver is even found into the substrate.

4. Discussion

The formation of spherical silver nanoparticles is evidenced from UV–visible optical absorption spectra, by an absorption band at 430 nm and it is then confirmed in both thermal and chemical treatments. Nevertheless, the difference of absorbance of the samples observed after respectively thermal and chemical treatments indicates that the chemical treatment induces a higher

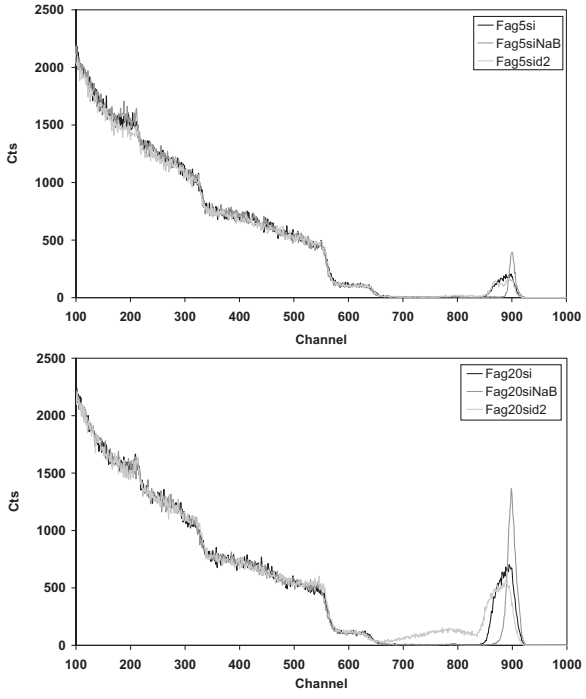

Fig. 8. Experimental RBS spectra of F127-silver-silica films.

density of silver nanoparticles in the film than the thermal treatment. By increasing the silver concentration from 5% to 20%, and by using a chemical treatment, an increase of absorbance from 0.45 to 0.71 is noted, since a higher concentration of silver nanoparticles is obtained. But, by using a thermal process, a broad absorption band appears at 510 nm, probably resulting from the superposition of two bands at around 420 and 570 nm. This is an indication of the existence of quadripolar effects in plasmon resonance, revealing the formation of non-spherical particles. Some authors [54,55] have reported that the growth of the band around 550 nm, concomitant with the decrease of the band at 400 nm, is explained by the conversion of spherical shaped particles into rectangular shaped particles.

The TEM experiments confirm the existence of spherical particles for the two Fag5Si samples. It reveals that an organized array of silver nanoparticles with ranging from 5 to 7 nm is obtained with a $NaBH_4$ treatment. The TEM images show that silver nanoparticles are formed without agglomeration because of the spatial control imposed by mesostructuration due to the block copolymer. On the other hand, in the case of thermal treatment, a lower density of silver nanoparticles randomly organized with size ranging from 8 to 12 nm is observed. For a higher silver concentration, TEM experiment reveals the formation of either spherical silver nanoparticles of about 7 nm for a $NaBH_4$ treatment, or, 40 nm long sticks for the thermally treated samples. The non-spherical form obtained in this last case explains the important red-shift of the visible absorption band. The growth of big nanoparticles, resulting from small nanoparticles fusion, is known as a ripening process already observed in silica films [21]. The ripening mechanism can be due to an Oswald process (atomic species from small particles are transported to larger particles) or to a particle migration and coalescence process (small particles migrate and coalesce) [56]. By considering the TEM images, we believe the second mechanism (particle migration and coalescence) is more likely involved. By comparing the nanoparticles obtained in the study of De et al. [21] with our results in the case of thermal reduction, it seems that the silver nanosticks are aligned in directions imposed by the mesostructure. It is not the case in a simple silica system, where the particles growth is occurring in random directions.

The SEM experiments reveal the existence of silver aggregates on the film surface before any reductive treatment. This is probably explained by the reductive ability of the block copolymer. The SEM images have shown that by using a chemical treatment large aggregates are formed at the film surface, while, on the other hand, by using a thermal treatment, the disappearance of silver aggregates from the film surface is noted.

Small-angle XRD results have shown that an increase in the silver salt concentration from 5% to 20% provokes a lower organization of the film mesostructure along the perpendicular direction to the substrate, since low-angle diffraction peaks are no more observable. XRD experiments have confirmed the formation of metallic silver.

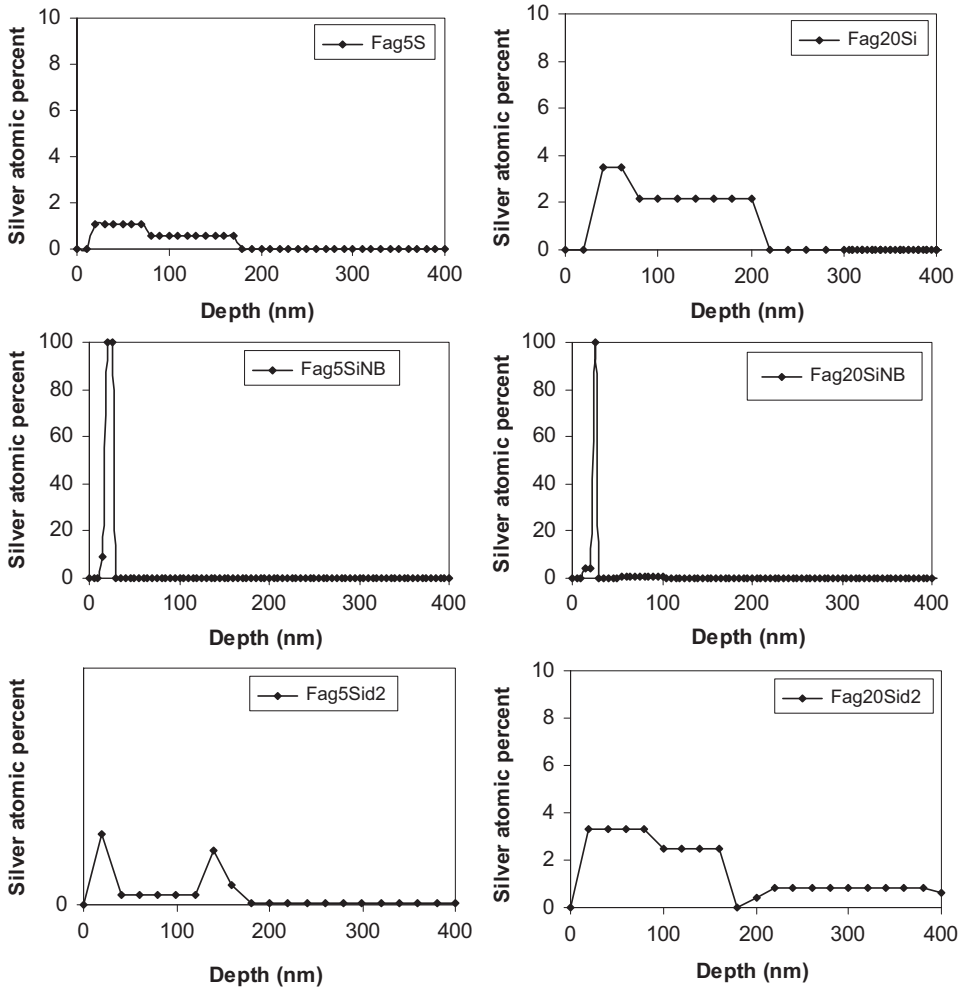

Fig. 9. Silver atomic concentration profile from the simulations of RBS spectra of F127-silver-silica films.

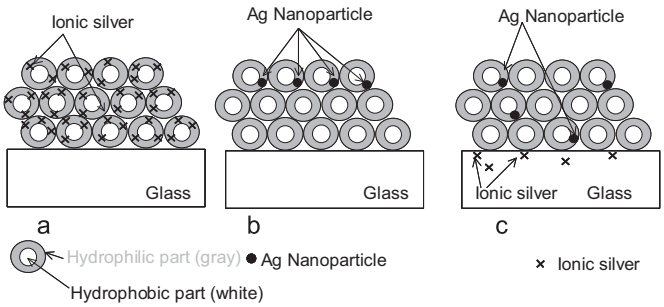

Fig. 10. Schematic representation of the mesostructured films a: before the reductive treatment; b: after $NaBH_4$ treatment; c: after thermal treatment at 200 °C.

RBS analysis allows to determine the silver profile in the film during the different steps. The intensive silver surface enrichment is evidenced after the chemical treatment and the migration of silver to the substrate during the thermal treatment is also demonstrated (Figs. 9 and 10).

A comparison between the chemical and the thermal reduction can now be drawn. We have shown that by performing a $NaBH_4$ process within a silica-block copolymer layer containing a silver salt, spherical silver nanoparticles with 10 nm diameter are formed. Moreover, the repartition of these silver nanoparticles is unordinary since they are located exclusively in the upper-side part of the mesotructure layer. This repartition can be understood by the very rapid nucleation of silver nanoparticles near the surface of the layer (during 5 s) [57]. This rapid nucleation could be followed by an aggregative growth involving diffusion of ionic silver or of small silver clusters from the depth of the layer to the nuclei, as it is discussed in another paper [46]. Within this sub-surface layer, silver nanoparticles are confined by the silica-block copolymer mesostructure so that a 2D organization of silver nanoparticles is obtained by diffusion into a mesostructured block copolymer-silica film. When a thermal process is involved, very different results have been obtained, since spherical silver nanoparticles are formed within the all depth of the layer (about 200 nm). Moreover, for higher silver level, the coalescence of spherical nanoparticles becomes possible, and silver nanosticks (long of 40 nm) are formed. At the end, the organization of these silver nanosticks is not arbitrary since a common orientation is evidenced by microscopy. It means that the migration of silver nanoparticles is directional and is also strongly influenced by the layer mesostructure. These materials constituted either of a 2D array of spherical nanoparticles at the sub-surface of a silica-polymer nanocomposite or of organized silver nanosticks within the same nanocomposite could both find some interest for their optical properties.

5. Conclusion

In summary, the growth of silver nanoparticles in mesostructured block copolymer F127-silica film has been studied by two processes: a chemical route involving $NaBH_4$ reduction and a thermal method. Spherical nanoparticles with diameter ranging from 5 to 8 nm are regularly disposed into the first layer of the mesostructured silica film by using the chemical route. The silver nanoparticles are preferentially formed at the film sub-surface (depth of 10 nm) and a 2D array is constituted by this way. The thermal route has allowed the formation, by migration and coalescence of spherical nanoparticles, of about 40 nm long silver sticks which are also regularly dispersed into the film mesostructure (depth 200 nm), conferring particular optical properties to this material. These results show that the block copolymer has a complex role since it contributes both to the reduction of silver ions, to the stabilisation of the silver nanoparticles and to their organization.

Acknowledgments

R. Vera (Centre de Diffractométrie Henri Longchambon, Université Claude Bernard Lyon 1, France) is sincerely acknowledged for his help in X-ray diffraction measurements. This work is supported by the ANR POMESCO project. Y.B. acknowledges the Région Rhône Alpes for financial support.

References

[1] M. Geissler, Y.N. Xia, Adv. Mater. 16 (2004) 1249.
[2] P. Mulvaney, Langmuir 12 (1996) 788.
[3] S.A. Maier, M.L. Brongersma, P.G. Kik, S. Meltzer, A.A.G. Requicha, H.A. Atwater, Adv. Mater. 13 (2001) 1501.
[4] A.N. Shipway, I. Willner, Chem. Commun. (2001) 2035.
[5] S.R. Nicewarner-Penä, R.G. Freeman, B.D. Reiss, L. He, D.J. Penä, I.D. Walton, C.D. Keating, M.J. Natan, Science 294 (2001) 137.
[6] M.S. Hu, H-L. Chen, C.H. Shen, L-S. Hong, B-R. Huang, K-H. Chen, L.-C. Chen, Nat. Mater. 5 (2006) 102.
[7] I. Ruach-Nir, T.A. Bendikov, I. Doron-Mor, Z. Barkay, A. Vaskevich, I. Rubinstein, J. Am. Chem. Soc. 129 (2007) 84.
[8] Y. Cong, J. Fu, Z. Zhang, Z. Cheng, R. Xing, J. Li, Y. Han, J. Appl. Polym. Sci. 100 (2006) 2737.
[9] S. Förster, T. Plantenberg, Angew. Chem. Int. Ed. 41 (2002) 688.
[10] I.W. Hamley, Angew. Chem. Int. Ed. 42 (2003) 1692.
[11] R.D. Deshmukh, G.A. Buxton, N. Clarke, R.J. Composto, Macromolecules 40 (17) (2007) 6316.
[12] L. Bronstein, E. Kraemer, B. Berton, C. Burger, S. Foerster, M. Antonietti, Chem. Mat. 11 (6) (1999) 1402.
[13] T. Thurn-Albrecht, J. Schotter, G.A. Kastle, N. Emley, T. Shibauchi, L. Krusin-Elbaun, K. Guarini, C.T. Black, M.T. Tuominen, T.P. Russell, Science 290 (5499) (2000) 2126.
[14] T. Sakai, P. Alexandridis, Chem. Mat. 18 (2006) 2577.
[15] L. Wang, X. Chen, J. Zhao, Z. Sui, W. Zhuang, L. Xu, C. Yang, Colloids Surf. A Physicochemical Eng. Aspects 231 (2005) 257–258.
[16] M. Malenovska, S. Martinez, M-A. Neouze, U. Schubert, Eur. J. Inorg. Chem. 18 (2007) 2609.
[17] K. Yliniemi, P. Ebbinghaus, P. Keil, K. Kontturi, G. Grundmeier, Surf. Coat. Technol. 201 (18) (2007) 7865.
[18] B.-H. Choi, H-H. Lee, S. Jin, S. Chun, S-H. Kim, Nanotechnology 18 (7) (2007) 075706/1–075706/5.
[19] A. Babapour, O. Akhavan, A.Z. Moshfegh, A.A. Hosseini, Thin Solid Films 515 (2) (2006) 771.
[20] A. Babapour, O. Akhavan, R. Azimirad, A.Z. Moshfegh, Nanotechnology 17 (3) (2006) 763.
[21] S. De, G. De, J. Mat. Chem. 16 (31) (2006) 3193.
[22] H. Jia, J. Zeng, W. Song, J. An, B. Zhao, Thin Solid Films 496 (2) (2006) 281.
[23] S. Pal, G. De, Chem. Mat. 17 (24) (2005) 6161.
[24] K. Kurihara, C. Rockstuhl, T. Nakano, T. Arai, J. Tominaga, Nanotechnology 16 (9) (2005) 1565.
[25] S. Shibata, K. Miyajima, Y. Kimura, T. Yano, J. Sol–Gel Sci. Technol. 31 (1/2/3) (2004) 123.
[26] A.A. Scalisi, G. Compagnini, L. D'Urso, O. Puglisi, Appl. Surf. Sci. 226 (1–3) (2004) 237.
[27] W. Li, S. Seal, E. Megan, J. Ramsdell, K. Scammon, G. Lelong, L. Lachal, K.A. Richardson, J. Appl. Phys. 93 (12) (2003) 9553.
[28] A.L. Pan, H.G. Zheng, Z.P. Yang, F.X. Liu, Z.J. Ding, Y.T. Qian, Mater. Res. Bull. 38 (5) (2003) 789.
[29] S.K. Mandal, R.K. Roy, A.K. Pal, J. Phys. D Appl. Phys. 36 (3) (2003) 261.
[30] Y. Sarov, M. Nikolaeva, M. Sendova-Vassileva, D. Malinovska, J.C. Pivin, Vacuum 69 (1–3) (2002) 321.
[31] S.K. Mandal, R.K. Roy, A.K. Pal, J. Phys. D Appl. Phys. 35 (17) (2002) 2198.
[32] Y.K. Mishra, S. Mohapatra, D. Kabiraj, B. Mohanta, N.P. Lalla, J.C. Pivin, D.K. Avasthi, Scr. Materialia 56 (7) (2007) 629.

[33] L. Guo, W. Liu, D. Liu, H. Tong, J. Lei, J. Wuhan Univ. Technol., Mater. Sci. Ed. 22 (4) (2007) 657.
[34] G. Valverde-Aguilar, V. Renteria, J.A. Garcia-Macedo, in: Proceedings of SPIE—The International Society for Optical Engineering, vol. 6641, 2007 (Plasmonics: Metallic Nanostructures and Their Optical Properties V).
[35] O. Dag, O. Samarskaya, N. Coombs, G.A. Ozin, J. Mat. Chem. 13 (2) (2003) 328.
[36] S. Besson, T. Gacoin, C. Ricolleau, J.-P. Boilot, Chem. Commun. (3) (2003) 360.
[37] C. Renard, C. Ricolleau, E. Fort, S. Besson, T. Gacoin, J.P. Boilot, Appl. Phys. Lett. 80 (2) (2002) 300.
[38] Y. Plyuto, J.M. Berquier, C. Jacquiod, C. Ricolleau, Chem. Commun. (1999) 1653.
[39] T. Gacoin, S. Besson, J.P. Boilot, J. Phys. Condens. Matter. 18 (2006) S85.
[40] J.A. Garcia-Macedo, G. Valverde, J. Lockard, J.I. Zink, in: Proceedings of SPIE—The International Society for Optical Engineering, vol. 5361, 2004 (Quantum Dots, Nanoparticles, and Nanoclusters), p. 117.
[41] J. Garcia-Macedo, A. Franco, G. Valverde, J.I. Zink, in: Proceedings of SPIE—The International Society for Optical Engineering, vol. 5520, 2004 (Organic Photovoltaics V), pp. 206–215.
[42] S. Eustis, G. Krylova, N. Smirnova, A. Eremenko, C. Tabor, W. Huang, M.A. El-Sayed, J. Photochem. Photobiol. A Chem. 181 (2–3) (2006) 385.
[43] G. Krylova, A. Eremenko, N. Smirnova, S. Eustis, Int. J. Photoenergy 7 (4) (2005) 193.
[44] G.V. Krylova, A.M. Eremenko, N.P. Smirnova, S. Eustis, Theor. Exp. Chem. 41 (2) (2005) 105.
[45] L. Bois, F. Bessueille, F. Chassagneux, Y. Battie, N. Destouches, C. Hubert, A. Boukenter, S. Parola, Colloids Surf. A Physicochem. Eng. Aspects 325 (2008) 86.
[46] N. Destouches, Y. Battie, Y. Ouerdane, A. Boukenter, L. Bois, F. Chassagneux, S. Parola, N. Moncoffre, N. Toulhoat, submitted for publication
[47] S. Dourdain, J.F. Bardeau, M. Colas, B. Smarsly, A. Mehdi, B.M. Ocko, A. Gibaud, Appl. Phys. Lett. 86 (2005) 11.
[48] A. Gibaud, M.J. Henderson, M. Colas, S. Dourdain, J.-F. Bardeau, J.W. White Journal of Nanotechnology On Line.
[49] M. Mayer, SIMNRA™ user's guide, Technical Report IPP 9/113, Max Planck Institute für Plasmaphysik Garching, 1997.
[50] H. Fang, M. Zhang, W.-H. Shi, T.-L. Wan, J. Non-Cryst. Sol. 352 (2006) 2279.
[51] S. Besson, C. Ricolleau, T. Gacoin, C. Jacquiod, J.P. Boilot, Microporous Mesoporous Mater. 60 (2003) 43.
[52] X. Jiang, Y. Xie, J. Lu, L. Zhu, W. He, Y. Qian, Langmuir 17 (2001) 3795.
[53] W. Li, S. Seal, E. Megan, J. Ramsdell, K. Scammon, G. Lelong, L. Lachal, K.A. Richardson, J. Appl. Phys. 93 (12) (2003) 9553.
[54] A. Sarkar, S. Kapoor, T. Mukherjee, J. Phys. Chem. B 109 (16) (2005) 7698.
[55] J.J. Mock, M. Barbic, D.R. Smith, D.A. Schultz, S. Schultz, J. Chem. Phys. 116 (2002) 15.
[56] L. Zhu, G. Lu, S. Mao, J. Chen, D.A. Dikin, X. Chen, R.S. Ruoff, NANO Brief Rep. Rev. 2 (3) (2007) 149.
[57] D.L. Van Hyning, W.G. Klemperer, C.F. Zukoski, Langmuir 17 (11) (2001) 3128.